Assessing and Improving the Quality of Unattended Radiation Observations in Antarctica

MICHIEL VAN DEN BROEKE, DIRK VAN AS, CARLEEN REIJMER, AND RODERIK VAN DE WAL

Institute for Marine and Atmospheric Research, Utrecht University, Utrecht, Netherlands

(Manuscript received 11 December 2003, in final form 18 March 2004)

ABSTRACT

The quality of atmospheric radiation measurements made at automatic weather stations (AWSs) in Antarctica is assessed. The AWSs are placed on the coastal ice shelf in the katabatic wind zone and on the high Antarctic plateau, and they measure shortwave and longwave radiation fluxes using unheated/unventilated Kipp and Zonen (KZ) CM3/CG3 sensors. During three summertime Antarctic experiments, the AWS sensors were directly compared to instruments of a higher standard, the KZ CM11 for shortwave and Eppley PIR for longwave radiation. It was found that the single-domed KZ CM3 is less sensitive to riming than the double-domed KZ CM11. With an accuracy better than 5% for daily averages, the KZ CM3 and CG3 perform better than their specifications. Net shortwave radiation calculated from individual pairs of incoming and reflected fluxes shows large relative errors, and a method is presented to remedy this. Summertime longwave fluxes measured with the KZ CG3 show very good agreement with ventilated Eppley PIR measurements [root-mean-square difference (rmsd) about 1%], but a larger systematic difference is found when comparison is made with unventilated Eppley PIR measurements. Upward extrapolation of snow temperatures suggest that the unventilated Eppley PIR measurements have a systematic offset, but additional measurements are necessary to confirm this. Wintertime riming of the unventilated/unheated KZ CG3 sensor window leads to rejection of 25%–28% of the LW$\downarrow$ data for the AWS on the ice shelf and the plateau. Replacing these data with parameterized values removes the systematic offset but introduces an uncertainty of 10%–15%.

1. Introduction

The surface radiation balance can be written as

$$\begin{aligned} R_{\text{net}} &= \text{SHW}_{\text{net}} + \text{LW}_{\text{net}}, \\ &= \text{SHW}\downarrow + \text{SHW}\uparrow + \text{LW}\downarrow + \text{LW}\uparrow, \\ &= \text{SHW}\downarrow(1 - \alpha) + \varepsilon\text{LW}\uparrow - \varepsilon\sigma T_s^4, \end{aligned} \quad (1)$$

where fluxes toward the surface are defined as being positive; R_{net} is the net radiation absorbed at the surface; SHW$\downarrow$, SHW$\uparrow$, LW$\downarrow$, and LW$\uparrow$ are the downwelling and upwelling fluxes of shortwave and longwave radiation, α is the spectrally integrated surface albedo defined as $\alpha = |\text{SHW}\uparrow|/\text{SHW}\downarrow$ (from now on referred to as ''albedo''); ε is the spectrally integrated surface emissivity for longwave radiation; σ is the Stefan–Boltzmann constant; and T_s is the surface temperature.

Reliable measurements of the radiation balance at the surface of the Antarctic ice sheet are important to assess its role as heat sink in the climate system of the earth, to serve as ground truth for satellite observations (e.g., to distinguish between clouds and the snow surface) and as validation for atmospheric models (King and Connolley 1997). They may also serve to develop albedo parameterizations for dry snow for use in atmospheric models or, more generally, as radiation parameterizations for energy and mass balance models (Konzelmann et al. 1994) and ice dynamical models (Van de Wal and Oerlemans 1997). Finally, a reliable assessment of the surface energy balance is not possible without accurate measurement of the radiation components (Bintanja and van den Broeke 1995; Van As et al. 2004, manuscript submitted to *Bound.-Layer Meteor.,* hereafter VAN04).

In Antarctica, reliable, year-round radiation balance measurements can only be made at manned stations, with daily maintenance and a continuous power supply for heating and ventilation of the sensors. At present, three Antarctic scientific stations are part of the Baseline Surface Radiation Network (BSRN) (Ohmura et al. 1998): Neumayer, Syowa, and South Pole (Fig. 1). Apart from these monitoring sites, short-term radiation observations in Antarctica have been made in several dedicated meteorological experiments (e.g., Liljequist 1956; Kuhn et al. 1977; King et al. 1989; König-Langlo and Augstein 1994; King 1996; Walden et al. 1998; Bintanja 2000; Van den Broeke et al. 2002). All in all,

Corresponding author address: Dr. Michiel van den Broeke, Institute for Marine and Atmospheric Research, Utrecht University, P.O. Box 80005, 3508TA Utrecht, Netherlands.
E-mail: broeke@phys.uu.nl

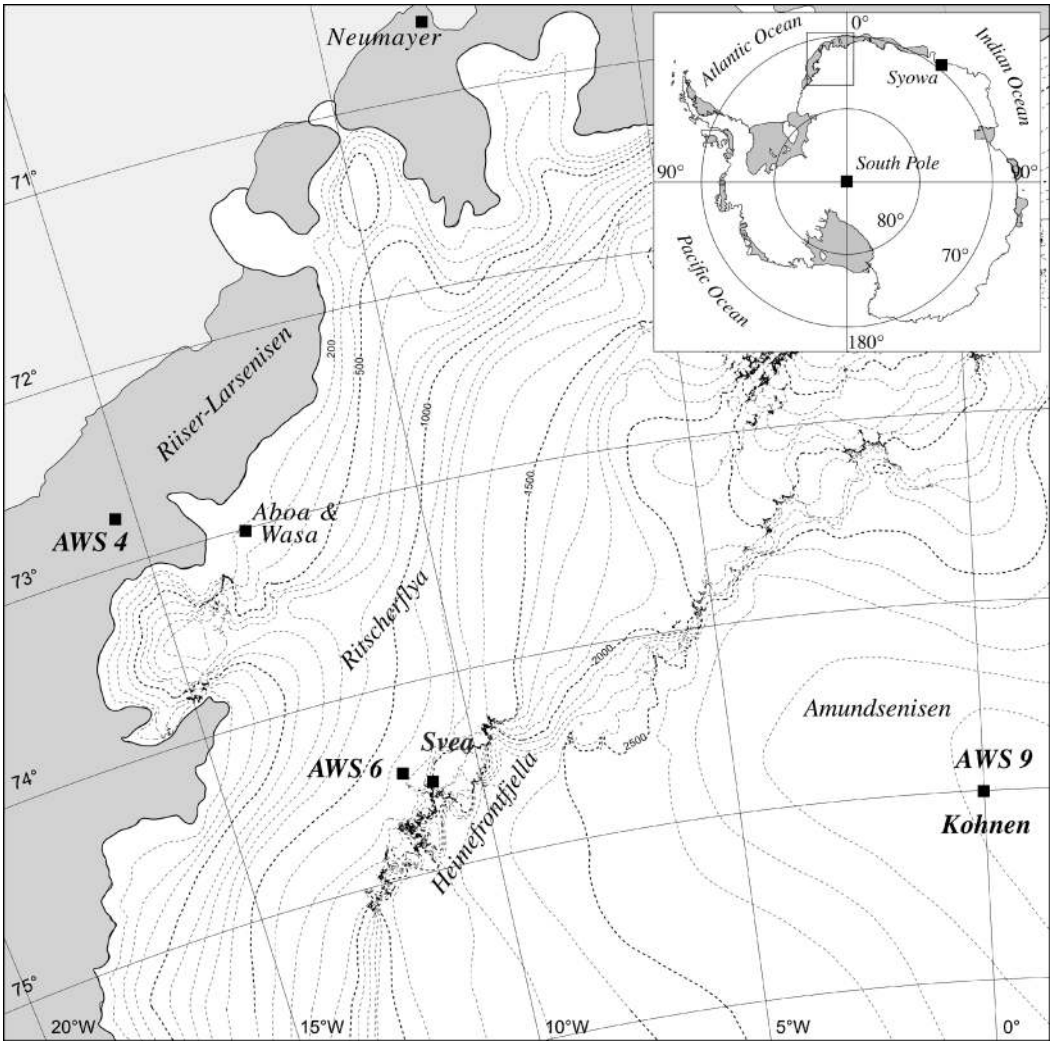

FIG. 1. Map of western Dronning Maud Land, Antarctica, with AWS and station locations, main topographical features, ice shelves (gray), and height contours (dashed lines, every 100 m).

the coverage of radiation measurements over Antarctica remains poor in space and time.

To fill in observational gaps, automatic weather stations (AWSs) have been proved to be invaluable for the study of Antarctic meteorology (Allison et al. 1993; Stearns and Wendler 1988; Reijmer and Oerlemans 2002; Renfrew and Anderson 2002). In 1997/98, an array of AWSs was installed in Dronning Maud Land, Antarctica, equipped with unventilated/unheated sensors to measure separately the four radiation components. In this paper we discuss the quality of these data and show how errors can be detected and accuracy improved using simple data treatment methods. In section 2 we briefly describe the experimental setup and the specifications of the radiation instruments. In section 3 and 4 we present results for shortwave and longwave radiation, followed by a summary in section 5.

2. Data and instrumentation

a. Description of AWSs and radiation sensors

We use radiation data of three AWSs in Dronning Maud Land, Antarctica, situated on the coastal ice shelf (AWS 4), in the katabatic wind zone (AWS 6), and on the polar plateau (AWS 9) (Fig. 1). A picture of AWS 9 is given in Fig. 2a with the radiation sensor enlarged in Fig. 2b. In an area with a radius of at least several kilometers around the AWS, the surface consists of snow. Some basic geographical and climatological information of the AWS is given in Table 1. The surface has a significant slope at AWS 6; the resulting katabatic wind climate is characterized by lower relative humidity, higher wind speed, and higher (surface) potential temperature (Bromwich 1989; van den Broeke et al. 1999). At AWS 4 and 9 the surface is nearly flat; here,

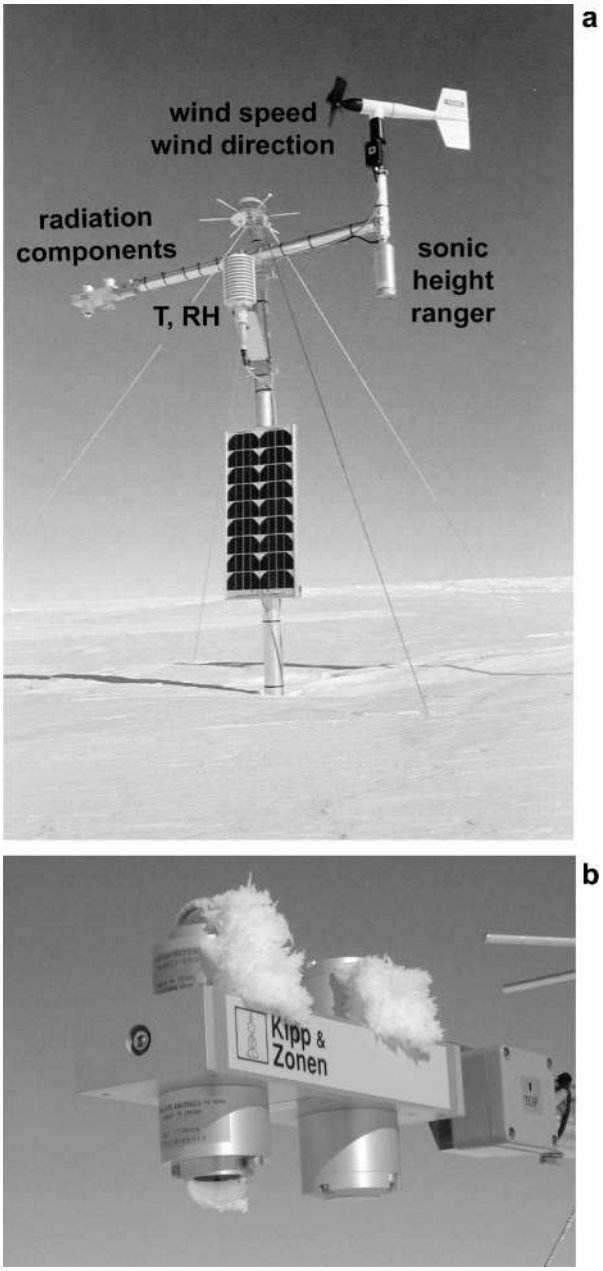

FIG. 2. (a) Picture of AWS 9. The datalogger and pressure sensor are buried in the snow; (b) enlarged image of KZ CNR1 radiation sensor.

wind speed and potential temperature are lower and relative humidity is higher.

The AWSs are equipped with Kipp and Zonen (KZ) CNR1 net radiometers (Fig. 2b). This sensor houses two KZ CM3 pyranometers for downward and upward broadband shortwave radiation flux (spectral range 305–2800 nm) and two KZ CG3 pyrgeometers for downward and upward broadband longwave radiation flux (spectral range of 5–50 μm). The KZ CM3 pyranometer is a thermopile-type pyranometer, covered by a single glass dome, which complies with ISO 9060 second-class specifications (estimated accuracy for daily totals $\pm 10\%$).

The KZ CG3 pyrgeometer consists of a thermopile sensor covered by a flat silicon window that is semitransparent for far-infrared radiation but absorbs solar radiation. The sensor output signal is a measure for the difference in radiation temperature between the sensor window and the object at which it looks. If both have the same temperature, the signal is zero. To obtain the absolute longwave radiation flux, the radiation flux emitted by the sensor window is added to the (calibrated) signal. The radiative temperature of the sensor window is assumed equal to the internal sensor body temperature, which is measured with a Pt-100 thermistor. No international standard exists for pyrgeometers; the factory-provided estimated accuracy of the KZ CG3 for daily totals is $\pm 10\%$.

A heating element is included in the sensor housing to prevent dew/rime deposition; this option is not used because this would deplete AWS batteries too rapidly at the low ambient temperatures encountered in Antarctica. The sampling interval for radiation at the AWS is 6 min, after which 2-h averages are calculated and stored in a Campbell CR10 datalogger. Because patchy clouds seldom occur in Antarctica, the relatively slow sampling rate does not cause problems, as will be demonstrated later.

From an operational point of view, we consider the KZ CNR1 a good choice for unattended use in Antarctica. Since the date of installation in 1997/98, out of a possible 1200 radiation component months (5 AWS $\times$ 5 yr $\times$ 12 months $\times$ 4 components), 88 radiation component months (7.3%) were lost of which nearly all (6.8%) were at a single AWS. For this paper, we use 4 yr (1998–2001) of uninterrupted radiation measurements of the other AWSs.

b. Comparison experiments

To assess the quality of the AWS radiation data, three comparison experiments were held in Antarctica, using KZ CM11 pyranometers and Eppley PIR pyrgeometers as reference sensors (Table 2). The KZ CM11 is an ISO secondary standard instrument with an estimated accuracy for daily totals of $\pm 3\%$. It has a double dome to prevent convection. The Eppley PIR measures body and dome temperature at three locations for improved determination of window radiation temperature. No factory-provided estimated accuracy is available for this sensor. Table 2 summarizes the location and period of the experiments and sensor specifications. During the Svea Cross experiment in 1998 (Bintanja 2000), reference measurements were performed close enough to AWS 6 to enable a direct comparison. At Kohnen in 2002, AWS 9 was too distant (1.7 km) for a direct comparison, and an AWS-type radiation sensor was included in the Kohnen radiation field (van den Broeke et al.

TABLE 1. Basic topographic and climate characteristics of AWS used in this study, 1998–2001.

	AWS 4	AWS 6	AWS 9
Start of observation	22 Dec 1997	15 Jan 1998	1 Jan 1998
End of observation	21 Dec 2001	14 Jan 2002	31 Dec 2001
Elevation (m ASL)	34	1160	2892
Surface slope (m km^{-1})	0.1	15.0	1.3
Temperature (K)	254.3	252.6	230.0
Potential temperature (K)	255.9	264.3	257.1
Relative humidity (%)	93	78	93
Specific humidity (g kg^{-1})	1.03	0.72	0.17
10-m wind speed (m s^{-1})	5.7	7.7	4.8

2002). At Neumayer in 2002, an AWS-type radiation sensor was installed 200 m south of the Neumayer radiation field. No AWS was nearby, but meteorological conditions at Neumayer, which is also situated on the ice shelf, are comparable to those at AWS 4 (Fig. 1). Neumayer is a BSRN station where the KZ CM11 and Eppley PIRs are artificially ventilated to prevent riming, which enhances the reliability of the reference observations at Neumayer. For the reference sensors, the sampling interval was 2 min at Svea Cross and 1 min at Kohnen and Neumayer. Two-hour and daily averages were calculated for comparison with the AWSs.

3. Results: Shortwave radiation

a. Typical problems affecting shortwave radiation measurements in Antarctica

1) ICING OF THE SENSOR DOME

Icing can occur when, during intrusions of warm and moist air masses (air temperature > -20°C), supercooled water droplets freeze upon impact with the dome of the radiation sensor (Fig. 2b). The upward-facing side of the sensor is more sensitive to icing than the underside, which is regularly freed from accreted ice due to the combined work of gravity and sensor arm vibrations. The relatively great thickness of the ice coating will generally lead to an underestimation of SHW↓. If we assume the measurement of SHW↑ to be unaffected, albedo $\alpha = |\text{SHW}\uparrow|/\text{SHW}\downarrow$ will be overestimated and SHW_{net} will be underestimated as a result of icing.

2) RIME FORMATION ON THE SENSOR DOME

Riming occurs when, *after* a warm air intrusion, the sky clears and the radiation instrument cools to space. This lowers the water vapor pressure at its surface and initiates water vapor transport from the air to the dome. The upward-looking sensor is most sensitive to riming, because it thermally equilibrates with the clear sky, while the downward-looking sensor dome ''sees'' the relatively warm snow surface. At low sun angles, the resulting thin ice coating diffracts sun rays onto the sensor plate, *overestimating* SHW↓ and, if the downward-looking sensor is not affected, underestimating α and overestimating SHW_{net}.

Figure 3a shows measured shortwave radiation fluxes at Kohnen on 18 January 2002, a day with riming conditions. Under a clear sky (0000–2000 UTC), riming increases SHW↓ of the KZ CM11 to values in excess of top-of-the-atmosphere (TOA) incoming radiation. Overcast conditions (from 2000 UTC onward) make the incoming radiation diffuse, and the detrimental effect of riming on SHW↓ disappears. Measurements of the KZ CM3 were not affected by riming on this day, which is no coincidence: at Kohnen, only 9% of the KZ CM3 data suffered from riming, while 72% of the KZ CM11 SHW↓ measurements had to be rejected because of riming problems. The single glass dome of the KZ CM3 is less susceptible to riming than is a double dome, because it is not thermally insulated from the black sensor plate beneath it. This allows it to heat up during periods of insolation, which prevents rime formation. For (unventilated and/or unheated) shortwave radiation observations on the Antarctic Plateau, a single-domed sensor is, thus, preferable. Riming was not observed on any upward-looking sensor at Svea Cross, where sublimation is a year-round feature owing to persistent katabatic winds (van den Broeke et al. 2004, unpublished manuscript). At Neumayer, artificial ventilation prevents riming of the reference instrument KZ CM11. The SHW↑ measurements are not noticeably affected by riming (Fig. 3a, only KZ CM3 shown) and none of the measurements at Kohnen had to be rejected.

3) LOW SUN ANGLE

The oblique angle under which the direct solar beam hits the horizontal sensor plate in Antarctica requires a good cosine response of the upward-looking sensor. This clearly poses a problem for the KZ CM3: in Fig. 3a, SHW↓ becomes smaller than SHW↑at low sun angles (0000–0230 UTC). Another problem associated with low sun angles is shading by nearby obstacles (see the spikes between 0300 and 0400 UTC in Fig. 3a). These problems do not occur when the radiation is isotropic, that is, for SHW↑ and under overcast conditions for SHW↓ (from 2000 UTC onward in Fig. 3a).

4) SENSOR TILT

When the upward-looking sensor is not aligned perfectly horizontally measured SHW↓ experiences a phase

TABLE 2. Summary of experiments and sensor specifications. KZ: Kipp and Zonen, ISO: International Standard Organization; E.a.d.t.: estimated accuracy of daily totals.

Location and period	Duration	Sensors used				Measurement interval	Notes
		Shortwave	Specification	Longwave	Specification		
AWS 4, 6, 9: 1997–2001	4 yr	KZ CM 3	ISO second class (e.a.d.t ±10%)	KZ CG 3	Factory provided e.a.d.t. ±10%	6-min, 2-h average stored ($N = 20$)	
Svea Cross: 14 Jan–7 Feb 1998	24 days	KZ CM11	ISO secondary standard (e.a.d.t. ±3%)	Eppley PIR	—	2-min, 2-h average for comparison with AWS ($N = 60$)	Direct comparison with AWS 6 possible
Kohnen: 7 Jan–8 Feb 2002	33 days	KZ CM11	ISO secondary standard (e.a.d.t. ±3%)	Eppley PIR	—	1-min, 2-h average for comparison with AWS ($N = 120$)	AWS 9 too distant (1.7 km) for direct comparison, an AWS-type sensor was included in the Kohnen radiation field.
Neumayer: 18–27 Feb 2002	9 days	KZ CM11 (ventilated)	ISO secondary standard (e.a.d.t. ±3%)	Eppley PIR (ventilated)	—	1-min, 2-h average for comparison with AWS ($N = 120$)	No AWS in vicinity; an AWS-type sensor was installed 200 m south of the Neumayer radiation field.

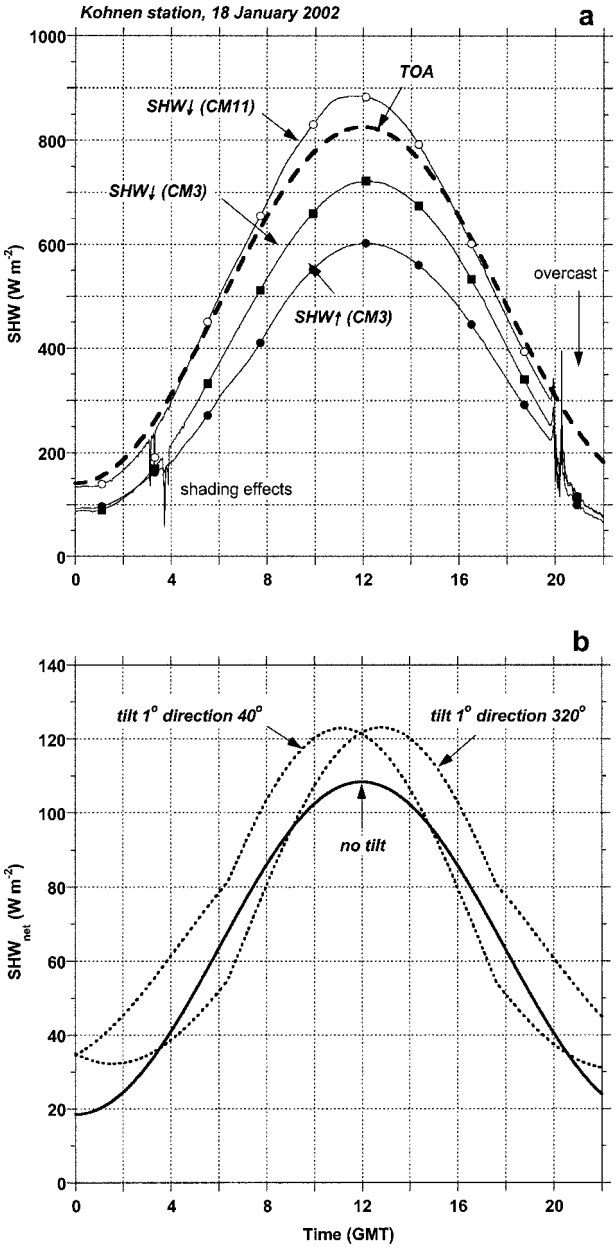

FIG. 3. (a) Incoming TOA (dashed line) and surface (SHW↓) shortwave radiation flux, and absolute value of reflected (SHW↑) shortwave radiative flux during on 18 Jan 2002, a day with riming at Kohnen. (b) Theoretical example of influence of sensor tilt on net shortwave radiation (SHW_{net}) for Julian day 18 at Kohnen. It is assumed that $\alpha = 0.85$ and that SHW↓ is not affected by the tilt.

shift, as well as a systematic error in daily totals. For SHW↑, which receives largely isotropic radiation, the associated error is given by the cosine of the tilt, which is negligible for tilt angles not exceeding several degrees. A theoretical example of how SHW_{net} is affected by tilt is given in Fig. 3b (calculated for Julian day 18 and the location of Kohnen station, 75°S, 0°) for a sensor leaning 1° toward the sun in the directions 40° and 320°, taking $\alpha = 0.85$ and neglecting the error in SHW↑. The

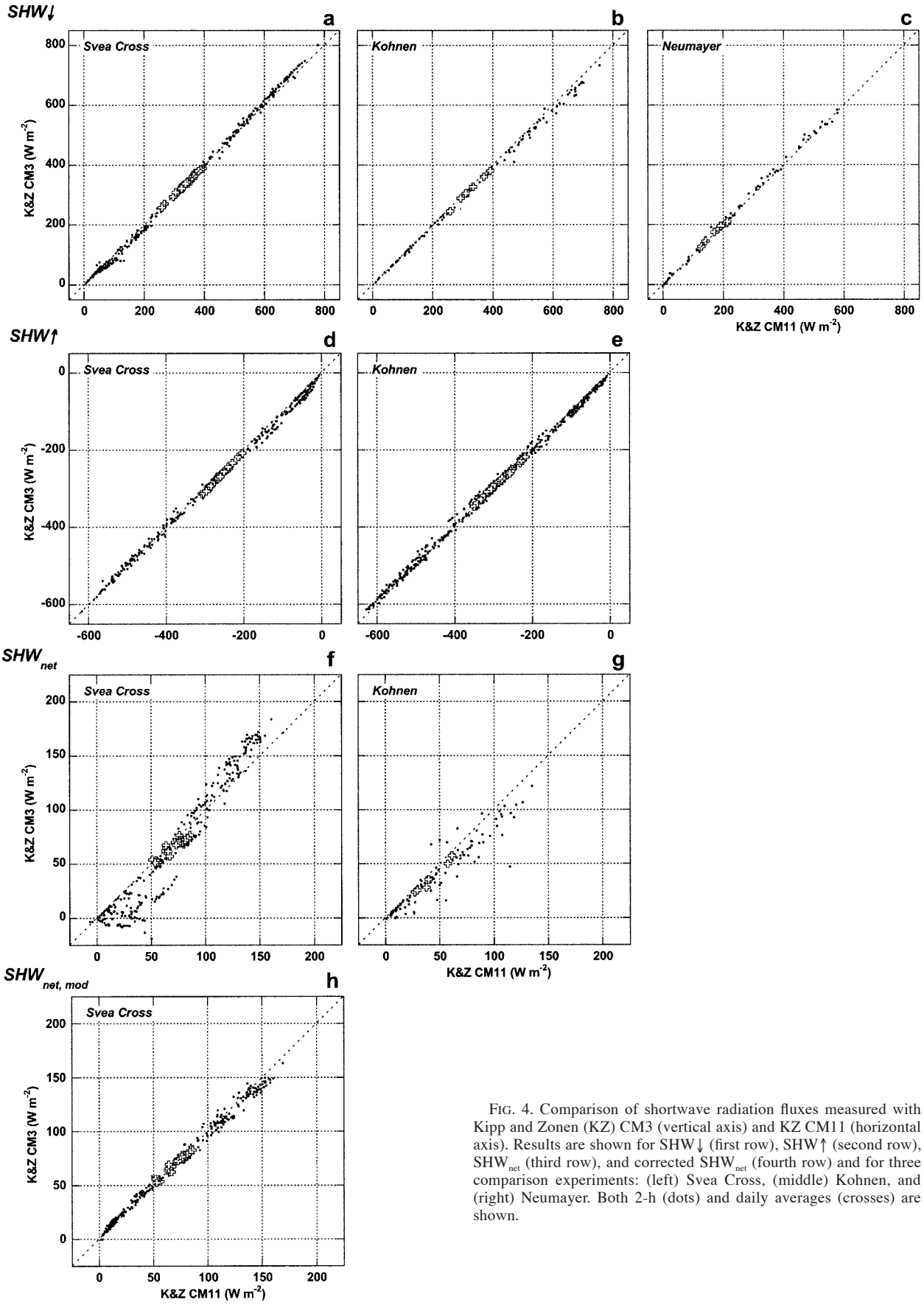

FIG. 4. Comparison of shortwave radiation fluxes measured with Kipp and Zonen (KZ) CM3 (vertical axis) and KZ CM11 (horizontal axis). Results are shown for SHW↓ (first row), SHW↑ (second row), SHW_{net} (third row), and corrected SHW_{net} (fourth row) and for three comparison experiments: (left) Svea Cross, (middle) Kohnen, and (right) Neumayer. Both 2-h (dots) and daily averages (crosses) are shown.

TABLE 3. Statistics of shortwave radiation comparisons of KZ CM3 with KZ CM11; N = number of points available for comparison. Listed average values (''Average'') are from KZ CM11. ''Difference'' is mean difference (KZ CM3 minus KZ CM11); Rmsd = root-mean-square difference.

		SHW↓				SHW↑				SHW_{net}			
Location	2-h/daily averages	N	Average ($W\ m^{-3}$)	Difference (%)	Rmsd (%)	N	Average ($W\ m^{-2}$)	Difference (%)	Rmsd (%)	N	Average ($W\ m^{-2}$)	Difference (%)	Rmsd (%)
Svea Cross	2 h	276	334.0	0.0	3.8	276	−263.2	−1.9	4.4	276	70.8	−6.1	26.6
												(0.0)*	(17.2)*
												(0.0)**	(6.9)**
	Daily	23	334.0	0.0	1.0	23	−263.2	−1.9	2.1	23	70.8	−6.1	8.8
												(0.0)*	(4.0)*
												(0.0)**	(3.2)**
Kohnen	2 h	110	339.6	−2.9	4.4	398	−289.5	1.0	3.8	110	48.1	−17.0	29.3
	Daily	6	325.4	−2.0	2.2	33	−290.3	1.0	1.4	6	41.9	−11.9	13.4
Neumayer	2 h	107	175.5	1.8	5.4	—	—	—	—	—	—	—	—
	Daily	8	177.2	1.7	2.7	—	—	—	—	—	—	—	—

* Only KZ CG3 time series corrected (see text).
** Both KZ CG3 and KZ CM11 corrected (see text).

tilt introduces a large relative error in SHW_{net} and a phase shift that breaks the symmetry around solar noon.

5) HIGH SURFACE ALBEDO

The four problems listed above mainly affect the measurement of SHW↓. In combination with a high surface albedo this greatly magnifies the *relative* uncertainty in SHW_{net}. Neglecting the error in SHW↑, the relative error in SHW_{net} can be expressed in terms of the relative error in SHW↓ and α:

$$\frac{\Delta(SHW_{net})}{SHW_{net}} = \frac{\Delta(SHW\downarrow)}{SHW\downarrow}\frac{1}{(1-\alpha)}. \quad (2)$$

For the tilt example in Fig. 3b, noontime values show a relative error in SHW_{net} of 12% for $\alpha = 0.85$, whereas for $\alpha = 0.15$ the relative error in SHW_{net} would be only 2%.

b. Shortwave radiation: Results of comparison experiments

Figures 4a–g compare SHW↓, SHW↑, and SHW_{net} measured using the KZ CM3 (vertical axis) and the KZ CM11 (horizontal axis) at the three sites. The graphs include 2-h averages (dots) as well as daily means (crosses). Table 3 lists for each site the number of observations used for the comparison, the average value (taken from the KZ CM 11), the average difference (KZ CM3 minus KZ CM 11), and the root-mean-square difference (rmsd); both the average difference and the rmsd are expressed as a percentages of the mean KZ CM 11 value.

The average differences for SHW↓ are less than ±3% for 2-h means and less than ±2% for daily means (Table 3). The rmsd is typically 4%–5% for 2-h means and 1%–3% for daily means. These values suggest a better performance of the KZ CM3 than the factory-provided ±10% for daily totals. Even under the conditions of strong insolation, absolute differences in SHW↓ in 2-h means are less than 15 $W\ m^{-2}$.

SHW↑ also shows good agreement (Figs. 4c,d). The average differences are less than ±2% for 2-h and daily means (Table 3). The rmsd is typically 4% for 2-h means and 1%–2% for daily means. Even under conditions of high radiation intensity, absolute differences in 2-h means are less than 10 $W\ m^{-2}$. No comparison of SHW↑ is made at Neumayer, where the sensors were placed about 200 m apart over a highly metamorphosed (late summer) snow surface, so that differences in surface albedo render a comparison of SHW↑ uncertain.

Calculating SHW_{net} from individual pairs of 2-h mean SHW↓ and SHW↑ results in large relative errors (Figs. 4f,g, Table 3). Differences in the average values are −6% to −17% for 2-h means and −6% to −12% for daily means. The rmsd is 27%–29% for 2-h means and 9%–13% for daily means. As was stated in section 3a, these large errors are caused by a combination of the following two factors: (a) the upward-facing pyranometer is more sensitive to measurement uncertainties than is the downward-facing sensor and (b) when the surface albedo is high, SHW_{net} is the difference between two large values.

Figure 5a highlights this problem for a sunny 3-day period at Svea Cross (28–30 January 1998). The TOA incoming radiation, scaled and offset for phase reference, is also shown. Large amplitude and phase differences in SHW_{net} occur between the time series of the KZ CM3 and CM11. Owing to a relatively poor cosine response, the KZ CM3 produces negative nighttime values of SHW_{net}, a feature that was also visible in the Kohnen data (see Fig. 3a). Neither the KZ CM3 nor the CM11 is in phase with TOA, which suggests phasing errors in both time series, probably due to sensor tilt. We conclude that calculating SHW_{net} from individual pairs of SHW↓and SHW↑results in unacceptably large errors. In the following section we propose a method to remedy this.

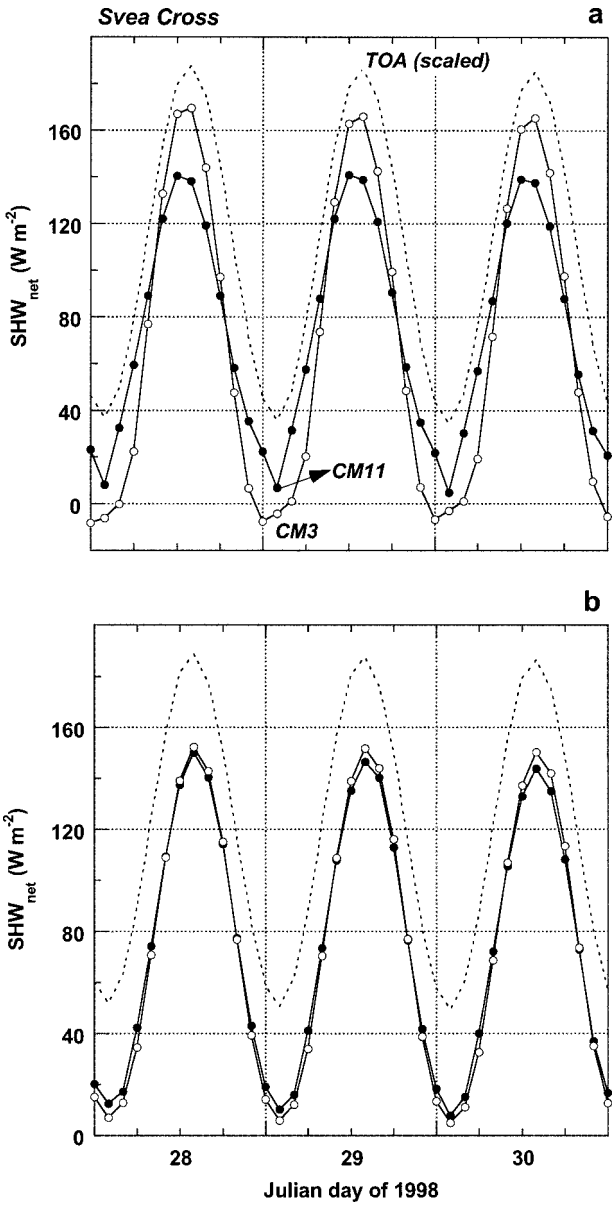

FIG. 5. (a) SHW_{net} for 3 days of fair weather at Svea Cross, as measured with the KZ CM3 and KZ CM11. SHW↓ at TOA is also shown, scaled and offset for comparison. (b) Same as (a), but after correction using the method of *accumulated albedo*.

c. A method to improve the accuracy of SHW_{net}

As previously stated in section 3a(5), SHW↑ is much less sensitive to measurement uncertainties than is SHW↓. This can be used to our advantage by choosing SHW↑ as the basis for the calculation of SHW_{net}:

$$\begin{aligned} SHW_{net} &= -SHW\uparrow(1 + \alpha)/\alpha \\ &\cong -SHW\uparrow(1 + \alpha_{acc})/\alpha_{acc}, \\ \alpha_{acc} &= \sum_{24\,h} |SHW\uparrow|/\sum_{24\,h} SHW\downarrow. \end{aligned} \tag{3}$$

Here, α_{acc} is an "accumulated" albedo, that is, the ratio of accumulated $|SHW\uparrow|$ and SHW↓ over a time window of 24 h centered around the moment of observation. In our case, α_{acc} is based on 2-h means, that is, 12 values. The underlying idea of this approach is that albedo changes due to snow metamorphism are likely to be small on subdaily time scales, while the use of α_{acc} largely eliminates errors in SHW↓ that are associated with a poor cosine response and phase shifts due to a possible tilt.

If we apply (3) to the KZ CM3 data only (assuming the KZ CM11 measurements to be accurate), statistics of SHW_{net} improve significantly (first number between brackets in last column of Table 3). However, agreement is best when we apply the method to both the KZ CM3 and KZ CM11 time series (second number between brackets in Table 3, Fig. 4h). The difference between the averages has vanished and the rmsd is reduced to 7% (4.9 W m^{-2}) for the 2-h means and 3% (2.3 W m^{-2}) for daily averages. Figure 5b shows that both the similarity between the time series and the phase compared to TOA have greatly improved. VAN04 show that the agreement of modeled and observed surface temperatures in an energy balance model significantly improves when the measured shortwave fluxes are treated in this fashion.

Another advantage of the accumulated albedo method is the robust value of α_{acc}, which allows for easy detection of riming and icing effects; rapid interdiurnal changes in the clear-sky value of α_{acc} or unlikely high/low α_{acc} values denote icing/riming problems that can be (automatically) removed or corrected.

An obvious disadvantage of the accumulated albedo method is that we have eliminated the clear-sky daily cycle in α. This daily cycle occurs as a result of the dependency of the diffuse fraction on solar zenith angle. This deficiency may be remedied by adding a theoretical daily cycle to α_{acc}, scaled such that the total daily SHW_{net} remains unchanged. Figure 6 shows an example of this procedure for a period of 3 months in the summer of 1998/99 at AWS 6. The upper line in Fig. 6a shows α_{acc} and the lower line is the added daily cycle calculated for a pure, semi-infinite snowpack using the model of Wiscombe and Warren (1980). This model needs snow grain size (here taken to be constant at 100 μm) and a diffuse fraction of SHW↓. The diffuse fraction was calculated using solar zenith angle and cloud cover estimated from observed net longwave radiation (Fig. 6b, lower line).

The resulting α_{acc} varies between 0.79 and 0.91. Clearly visible is the effect of clouds that change the spectrum of the shortwave radiation, reaching the surface and causing a profound increase of surface albedo (van den Broeke et al. 2004). The lowest value of α_{acc} is reached after a period of sustained clear and dry weather at the end of January 1999. Three precipitation events each bring 10–15 cm of fresh snow (Fig. 6b, upper line). After each snowfall event, the albedo increases and then exponentially decreases back to the baseline value. Note

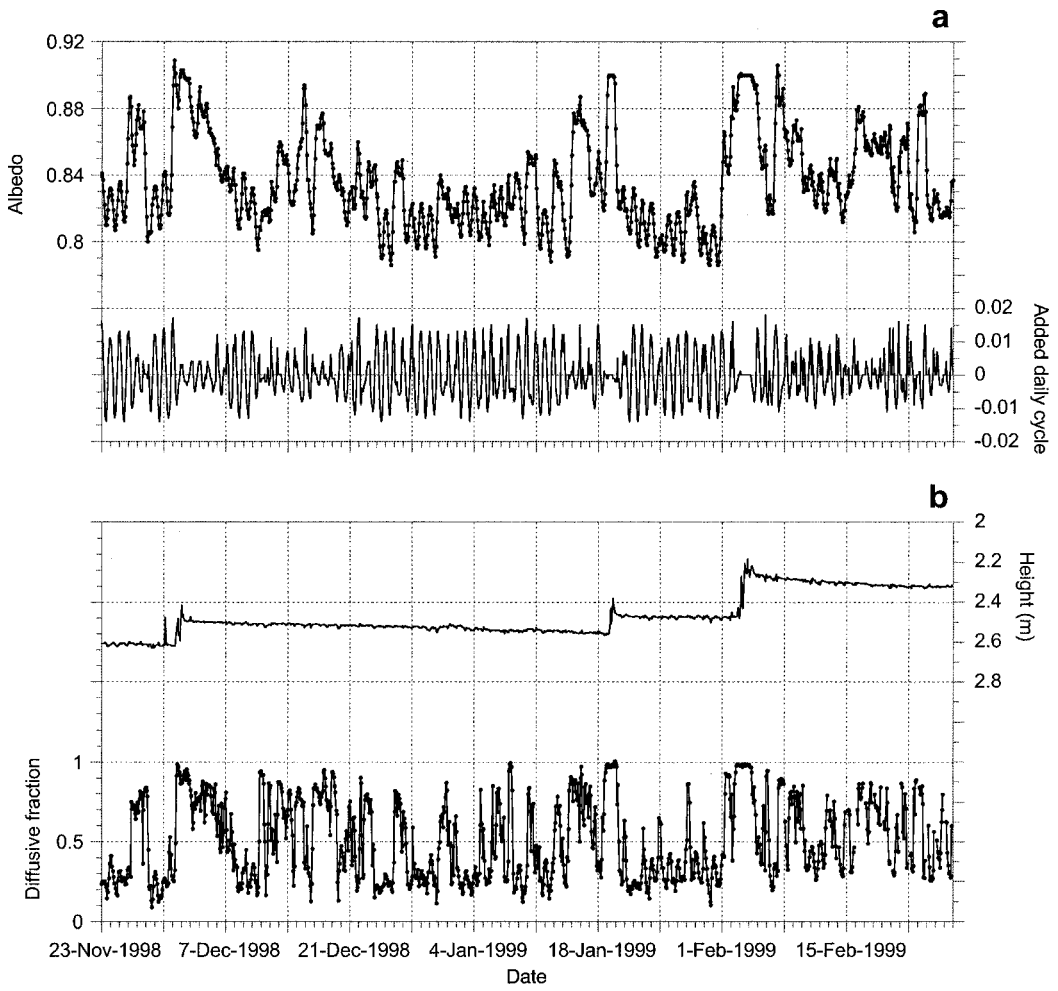

FIG. 6. (a) Accumulated albedo α_{acc} for a 3-month period in the summer of 1998/99 at AWS 6 (upper line) and added theoretical daily cycle (lower line). (b) Surface snow height (upper line, note inverted scale) and estimated diffusive fraction of incoming shortwave radiation (lower line).

that we have not added an artificial daily cycle to the albedo for the results presented in Figs. 4h and 5b.

4. Results: Longwave radiation

a. Typical problems affecting longwave radiation measurements in Antarctica

1) WINDOW HEATING OFFSET

A systematic measurement error is caused by absorption of solar radiation by the silicon window causing it to become warmer than the sensor housing. If the window temperature is not measured separately, we can not correct for this. This problem is most severe for the upward-facing KZ CG3 on sunny, windless days, and may produce a window heating offset of typically 25 W m^{-2} under 1000 W m^{-2} solar irradiance (numbers provided by the factory). This error can be minimized by shading and/or ventilation of the sensor, none of which is feasible for Antarctic AWSs.

2) RIMING OF THE UPWARD-FACING PYRGEOMETER WINDOW

A serious error is caused by wintertime riming of the upward-facing KZ CG3. Figures 7a–d show daily mean values of LW↓ (dots) and |LW↑| (upper line) at Neumayer and AWS 4, 6, and 9 for the period of 1998–2001 ($N = 1461$), as a function of the AWS temperature T. For all locations, LW↓ = |LW↑| (i.e., $LW_{net} = 0$) is a clear upper boundary; at high T this represents overcast conditions when the snow surface thermally equilibrates with the warm cloud base and vertical temperature gradients are small. The lower boundary represents clear-sky conditions with LW↓ < |LW↑| and a significant near-surface temperature inversion. Greatest negative values of LW_{net} occur during clear-sky conditions in summer, when absorption of shortwave radiation warms the snow surface (high T).

Obviously, a negative LW_{net} is required for low T to occur in winter because this is the only significant sur-

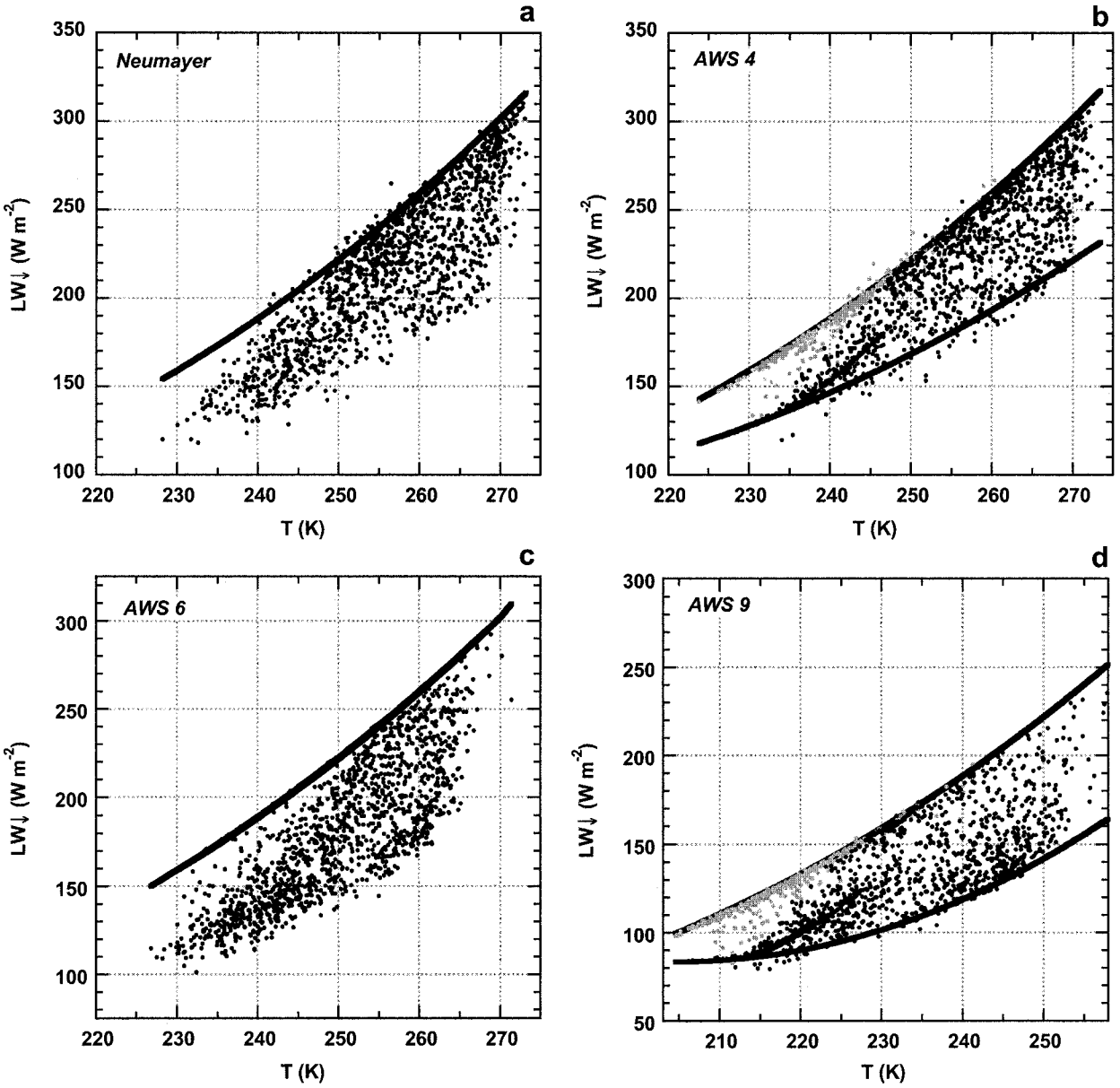

FIG. 7. Daily means of incoming (LW↓, dots) and absolute value of upwelling (LW↑, upper line) longwave radiative flux as a function of temperature T_s at (a) Neumayer, (b) AWS 4, (c) AWS 6, and (d) AWS 9. For AWS 4 and 9, the rejected data are in light gray. The fitted lower boundary for the parameterization of LW↓ (lower line) is included.

face heat sink. In Figs. 7a (Neumayer) and Fig. 7c (AWS 6) this is visible as a lack of points where LW↓ = |LW↑| at low T. At AWSs 4 and 9, the clustering of points around LW↓ = |LW↑| at low T (gray dots in Figs. 7b and 7d) represent measurement errors due to riming. The problem occurs only at AWSs 4 and 9, while riming neither affects measurements at Neumayer, where the sensors are ventilated, nor at AWS 6, where dry katabatic winds keeps the sensors free of ice (van den Broeke et al. 2004). Because rime completely obstructs the transmission of LW↓, the only way to solve this problem is to replace these data with parameterized values of LW↓ (see section d).

3) RIMING OF THE DOWNWARD-FACING PYRGEOMETER WINDOW

Riming of the downward-looking pyrgeometer window also occurs. This problem is less severe because owing to the proximity of the surface, sensor and snow surface temperatures will be similar. Nevertheless, to avoid a systematic bias during these periods we calculate

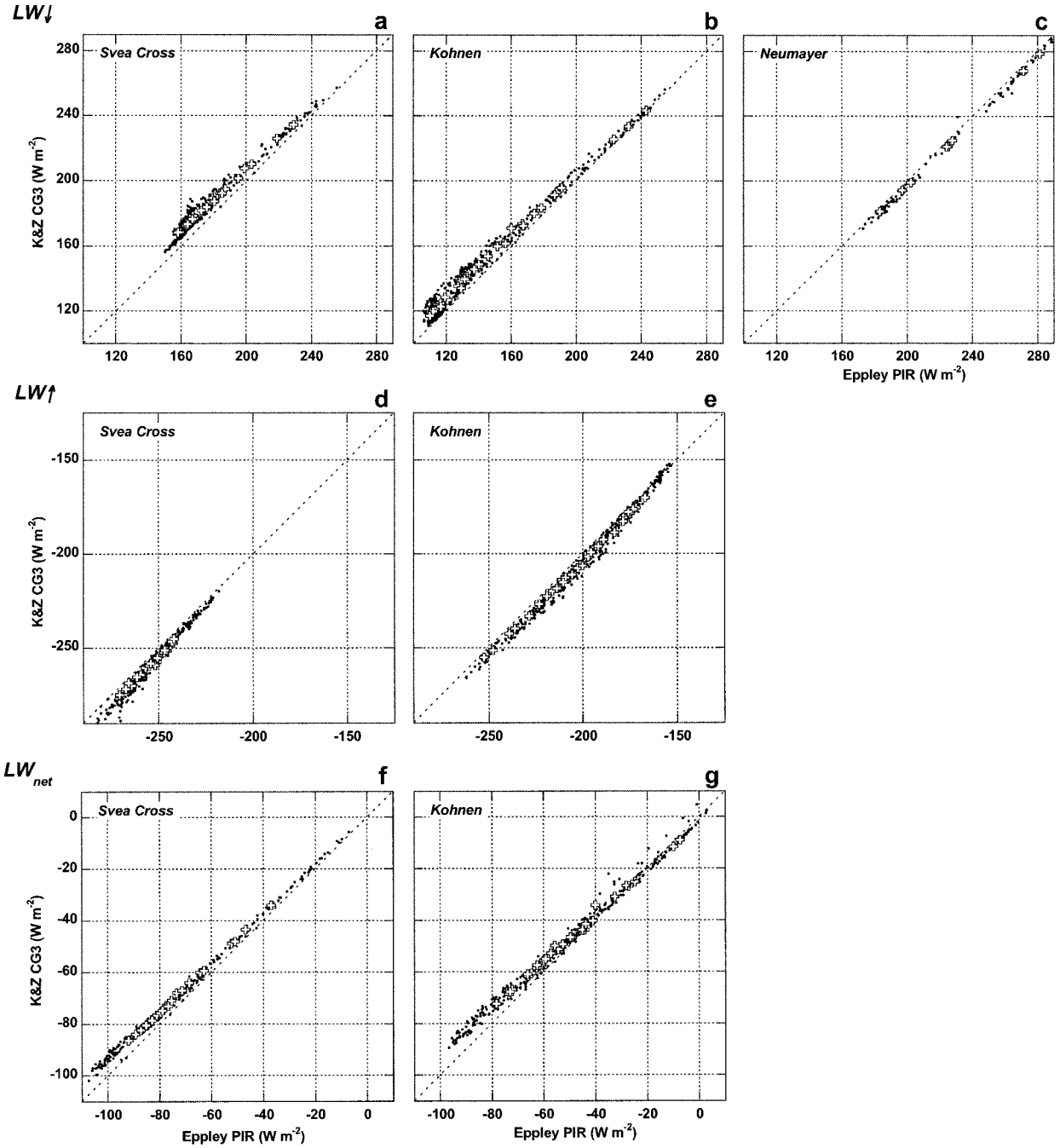

FIG. 8. Comparison of longwave radiation fluxes measured with KZ CG3 (vertical axis) and Eppley PIR (horizontal axis). Results are shown for LW↓ (first row), LW↑ (second row), and LW_{net} (third row) and for three comparison experiments: (left) Svea Cross, (middle) Kohnen, and (right) Neumayer. Both 2-h (dots) and daily (crosses) averages are shown.

the surface temperature (and hence LW↑) using an energy balance model.

b. Longwave radiation: Results of comparison experiments

Figures 8a–g compare LW↓, LW↑, and LW_{net} measured by the KZ CG3 (vertical axis) with the Eppley PIR (horizontal axis). Table 4 summarizes the results. During these summer experiments, riming did not significantly affect measurements of LW↓; for instance, only seven 2-h averages of LW↓ were rejected from the Kohnen data (Table 4).

Figures 8a–c show acceptable agreement between KZ CG3 and Eppley PIR for LW↓, although a systematic positive offset is found at Svea Cross and Kohnen, es-

TABLE 4. Statistics of longwave radiation comparisons of KZ CG3 with Eppley PIR; N = number of points available for comparison. Listed average values (''Average'') are from KZ CM11. ''Difference'' is mean difference (KZ CM3 minus KZ CM11); Rmsd is the root-mean-square difference.

		LW↓				LW↑				LW_{net}			
Location	2-h/daily averages	N	Average (W m^{-2})	Difference (%)	Rmsd (%)	N	Average (W m^{-2})	Difference (%)	Rmsd (%)	N	Average (W m^{-2})	Difference (%)	Rmsd (%)
Svea Cross	2 h	279	179.7	5.0	5.5	276	−253.3	−1.7	2.1	276	−73.6	6.1	6.7
	Daily	23	179.7	5.0	5.0	23	−253.3	−1.7	1.8	23	−73.6	6.1	6.1
Kohnen	2 h	391	150.2	4.6	5.7	398	−201.9	−1.8	2.3	391	−52.1	6.5	9.1
	Daily	31	151.5	4.5	4.8	33	−201.9	−1.8	1.8	31	−51.7	6.5	7.8
Neumayer	2 h	107	226.7	−1.1	1.5	—	—	—	—	—	—	—	—
	Daily	8	226.4	−1.1	1.2	—	—	—	—	—	—	—	—

pecially during clear-sky conditions (low LW↓). This could be the result of a window heating offset of the KZ CG3, but note that no such positive difference is found at Neumayer where the Eppley PIRs are ventilated. The differences in the average values are between −1% (Neumayer) to 5%–6% (Svea Cross) for 2-h and daily means (Table 4). The rmsd ranges between 1% (Neumayer) and 6% (Svea Cross). These values suggest a better performance of the KZ CG3 than that of the factory-provided estimated accuracy of ±10% for daily totals.

For LW↑ a similar but smaller systematic offset is found at Svea Cross and Kohnen (Figs. 8d and 8e), with the KZ CG3 giving a larger absolute signal than the Eppley PIR. The average differences and rmsds are smaller than for LW↓, typically 2% (Table 4). We did not include results for LW↑ at Neumayer, because of the distance between the measurement sites (200 m); we just state here that, as was the case for LW↓, excellent agreement is found for LW↑ with rmsd's less than 1%.

Because systematic errors are larger for LW↓ than for LW↑, LW_{net} suffers from fairly great relative uncertainty, up to 9% (Figs. 8f,g); however, the absolute differences are at most 8 W m^{-2} in 2-h averages and are generally better than 5 W m^{-2} for daily means.

c. Using snow temperatures to check LW↑

To see if the systematic offset in Figs. 8d and 8e can be explained, temperature measurements in the near-surface snowpack were used to check the measured LW↑. For a typical sunny period at Svea Cross, Fig. 9a shows T_s derived from observed LW↑, assuming that the snow surface has unit longwave emissivity

$$T_s = (\mathrm{LW}\uparrow)^{0.25}\sigma^{-0.25}, \quad (4)$$

where $\sigma = 5.67 \times 10^{-8}$ W m^{-2} K^{-4} is the Stefan–Boltzmann constant. Daytime T_s thus derived from the two sensors signals differ by up to 3.5 K at noon (corresponding to a difference in LW↑ of about 15 W m^{-2}). Also included in Fig. 9a are snow temperatures measured at depths $d = 0.05, 0.10, 0.20$, and 0.40 m (dashed lines). If we assume that the subsurface temperature wave is forced at the surface by T_s and travels in a homogenous medium, it must show the following characteristics: (a) a constant period with depth, (b) an exponentially decreasing amplitude with depth, and (c) an increase of phase with depth. Neither the phase nor the amplitude of the T_s time series derived from the Eppley PIR in Fig. 9a is consistent with this. We must assume a surface emissivity $\varepsilon = 0.90$ to obtain a consistent daily cycle in T_s from the Eppley PIR, which is clearly outside the range of ε values reported for clean, fine-grained snow (Wilber et al. 1999). The signal from the KZ CG3 appears to behave correctly.

Figure 9b shows the amplitude of the average daily temperature cycle as a function of depth d for the whole duration of the experiment at Svea Cross (from 15 January to 6 February 1998). When extrapolated toward $d = 0$, this gives the amplitude of T_s. The value, thus found, exactly matches that predicted by the KZ CG3 (9.4 K) but is significantly larger than that measured by the Eppley PIR (7.9 K). Similar results were found at Kohnen, which implies that the KZ CG3 measurement of LW↑ is correct. Clearly, measurement errors in snow temperatures due to shortwave radiation penetration cannot be ruled out, and the smaller incoming shortwave fluxes at Neumayer may have masked the problem there. More detailed comparison measurements are, therefore, needed to resolve this issue.

d. Obtaining LW↓ during riming episodes

Wintertime values of LW↓ and near-surface temperature T are strongly coupled, so that rejected LW↓ measurements at AWSs 4 and 9 may be replaced by parameterized values, using T as predictor. We developed a parameterization using the following procedure: first, a polynomial was fitted to the fifth percentile of LW↓ in 5-K intervals of T. This lower envelope of LW↓ represents clear-sky conditions and is shown in Figs. 7b and 7d. The upper envelope of LW↓ is simply assumed to equal |LW↑| and represents overcast conditions (included in Figs. 7a–d). Next, upper and lower envelopes were also constructed for the seasonal cycle of T by fitting polynomials to the 5th and 95th percentiles of daily average T, which was first binned in 0.08 intervals

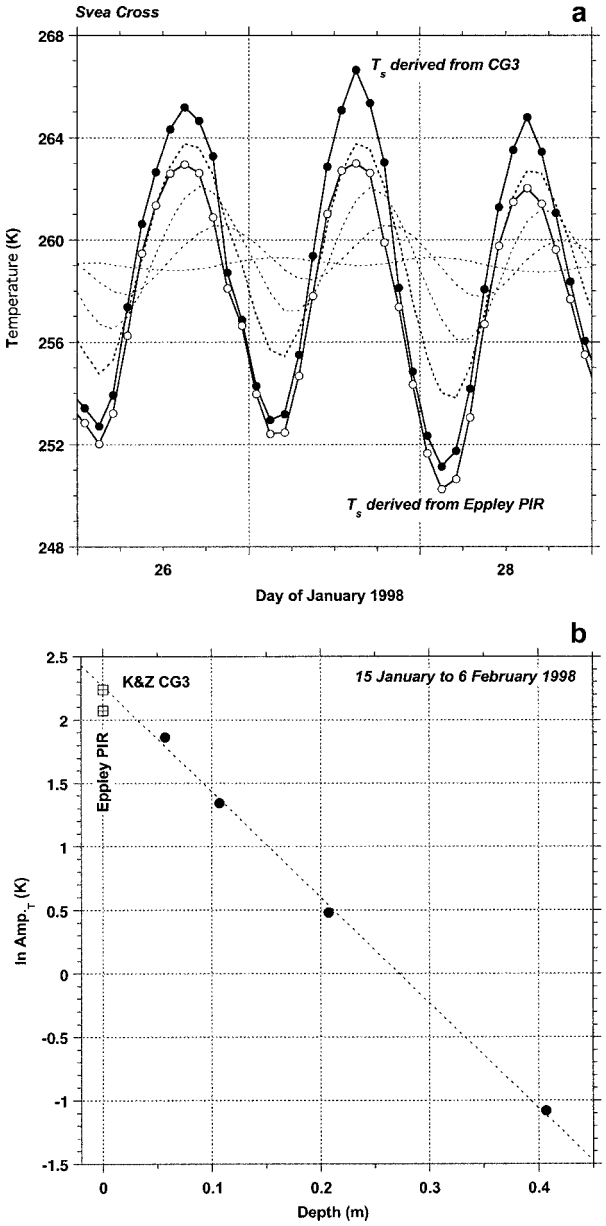

FIG. 9. (a) Svea Cross, 26–28 Jan 1998: surface temperature T_s derived from LW↑ (solid lines) and snow temperatures at 5-, 10-, 20-, and 40-cm depths (dashed lines). (b) Average amplitude of snow temperatures (15 Jan–6 Feb 1998) as a function of depth for the Svea Cross experiment.

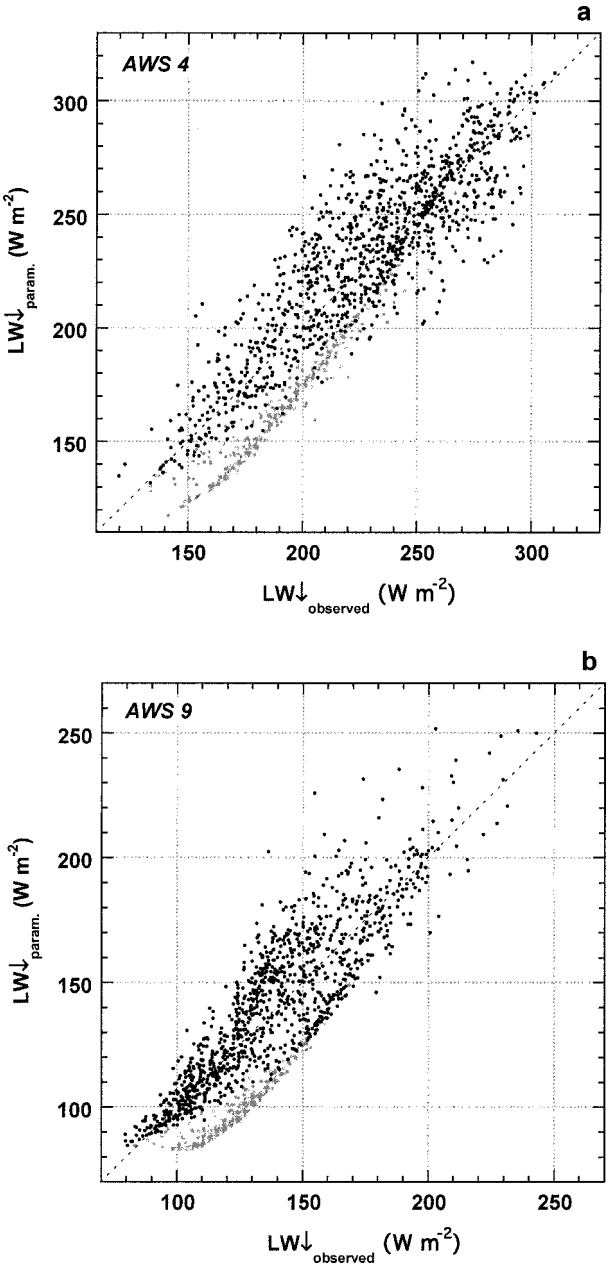

FIG. 10. Results of parameterization of daily averaged incoming longwave radiation LW↓ at (a) AWS 4 and (b) AWS 9. Rejected data are light gray.

of solar zenith angle (time of year). We connect LW↓ to T by assuming that changes in wintertime T are driven entirely by changes in LW_{net}. As the basis for the parameterization we chose rime-free data points.

Finally, we need a criterion to detect erroneous LW↓. For this we adopt a threshold value of T below which LW↓ = |LW↑| (i.e., $LW_{net} = 0$) is no longer accepted. Based on Fig. 7, we choose 250 K for AWS 4 and 230 K for AWS 9. This results in 25% and 28% LW↓ data rejection for AWSs 4 and 9 (rejected data are light colored in Figs. 7b and 7d). Although this selection method is rather crude, it should be noted that when ''good'' data points are accidentally rejected, the parameterized values that replace them should not be too far off.

For AWSs 4 and 9, the results of this parameterization are presented in Figs. 10a and 10b, respectively, where the rejected observations are presented as light gray symbols. As can be seen, clearly erroneous values have been removed and the remaining deviations are randomly distributed so that no systematic error remains.

It is favorable that scatter is smaller for the low LW↓ values, that is, the regime in which the parameterized values are used. For AWS 4 and $T < 250$ K, the parameterized values have an rmsd of 15 W m^{-2}; for AWS 9 and $T_s < 230$ K, the rmsd is 10 W m^{-2}. These values are larger than the rmsd listed in Table 4, but at least the systematic error is removed from the time series so that monthly means may now be calculated from the data (Van den Broeke et al. 2004).

5. Summary and conclusions

We assessed the quality of radiation observations from automatic weather stations (AWSs) in Antarctica. On the AWSs are deployed Kipp and Zonen (KZ) CM3 sensors for shortwave fluxes (SHW↓ and SHW↑) and KZ CG3 sensors for longwave fluxes (LW↓ and LW↑). Both sensors have estimated accuracies for daily totals of ±10%. We tested their performance in three summertime Antarctic experiments on the ice shelf (Neumayer base), in the katabatic wind zone (near Svea station), and on the Antarctic plateau (Kohnen base), using KZ CM11 and Eppley PIR as reference sensors. The main results for shortwave radiation are the following.

- The single-domed KZ CM3 is less susceptible to summertime riming than the double-domed KZ CM11, an important characteristic for sensors left unattended, unheated, and unventilated.
- Root-mean-squared differences (rmsd's) between 2-h averages ($N = 20$) of SHW↓ and SHW↑ are smaller than 5%, daily mean values ($N = 240$) have rmsd's smaller than 3%. This exceeds the specifications of the KZ CM3 (estimated accuracy ±10% for daily totals).
- If net shortwave radiation SHW_{net} is calculated from individual pairs of SHW↓ and SHW↑, rmsd's are unacceptably large (up to 30%). A method is proposed that improves the accuracy of SHW_{net} with a factor of 3 (daily means) to 4 (2-h averages).

The main results for longwave radiation are as follows.

- Very small rmsds of about 1% are found when the KZ CG3 is compared with a *ventilated* Eppley PIR at Neumayer. Rmsd's of 2%–6% are found when a comparison is made with unventilated Eppley PIR. Based on upward extrapolation of snow temperatures, the downward-facing Eppley PIR measurements appear to have a systematic offset, but additional measurements are necessary to quantify the role of, for example, a window heating offset in longwave radiation instruments in Antarctica.
- Overall, rmsd's of 2-h average values ($N = 12$) and daily means ($N = 144$) are better than factory-provided specifications of the KZ CG3 (estimated accuracy ±10% for daily totals).
- LW_{net} has a large rmsd of up to 9%, but in absolute sense is <5 W m^{-2}.
- Energy considerations prevent the use of the built-in sensor heater in the KZ CG3. As a result, riming during winter leads to a 25%–28% rejection of the KZ CG3 LW↓ data of the ice shelf and plateau AWSs. Substituting these with parameterized values of daily mean LW↓ removes the systematic offset but introduces an uncertainty of 10%–15%.

Owing to its reliability, overall good accuracy and favorable summertime riming characteristics, we conclude that the KZ CNR1 is suitable for unattended radiation observations in Antarctica. When energy is available, the heating option should be used to prevent riming during winter. When the data are checked and treated using the methods outlined in this paper, they should be sufficiently accurate to derive a radiation climatology from and/or to serve as ground truth for satellite measurements and boundary condition for energy balance calculations.

Acknowledgments. We wish to thank the IMAU technical department for the AWS development and support. Participants of SWEDARP'97/98 are thanked for setting up AWS 4, 5, and 6 and hosting the Svea experiment. We thank colleagues of the Alfred Wegener Institute for setting up and regular servicing of AWS 9, as well as hosting the Kohnen experiment. Use of the Neumayer radiation data is gratefully acknowledged. Field parties of IMAU and SWEDARP are thanked for maintenance work on AWS 4, 5, and 6. This work is partly funded by the Netherlands Antarctic Program (NAAP) and the Netherlands Organisation of Scientific Research, section on Earth and Life Sciences (NWO/ALW). Two anonymous reviewers and Wouter Greuell (IMAU) have provided comments that have improved the manuscript.

REFERENCES

Allison, I., G. Wendler, and U. Radok, 1993: Climatology of the East Antarctic ice sheet (100°E to 140°E) derived from automatic weather stations. *J. Geophys. Res.,* **98** (D5), 8815–8823.

Bintanja, R., 2000: Surface heat budget of Antarctic snow and blue ice: Interpretation of spatial and temporal variability. *J. Geophys. Res.,* **105** (D19), 24 387–24 408.

——, and M. R. van den Broeke, 1995: The surface energy balance of Antarctic snow and blue ice. *J. Appl. Meteor.,* **34,** 902–926.

Bromwich, D. H., 1989: Satellite analyses of Antarctic katabatic wind behavior. *Bull. Amer. Meteor. Soc.,* **70,** 738–749.

King, J. C., 1996: Longwave atmospheric radiation over Antarctica. *Antarct. Sci.,* **8,** 105–109.

——, and W. M. Connolley, 1997: Validation of the surface energy balance over the Antarctic ice sheets in the U.K. Meteorological Office Unified Climate Model. *J. Climate,* **10,** 1273–1287.

——, S. D. Mobbs, J. M. Rees, P. S. Anderson, and A. D. Cliff, 1989: The STABLE Antarctic boundary layer experiment at Halley station. *Weather,* **44,** 398–405.

König-Langlo, G., and E. Augstein, 1994: Parameterisation of the downward long-wave radiation at the Earth's surface in polar regions. *Meteor. Z.,* **3,** 343–347.

Konzelmann, T., R. S. W. van de Wal, W. Greuell, R. Bintanja, A.

A. C. Henneken, and A. Abe-Ouchi, 1994: Parameterisation of global and longwave incoming radiation for the Greenland ice sheet. *Global Planet. Change,* **9,** 143–164.

Kuhn, M., H. H. Lettau, and A. J. Riordan, 1977: The radiation budget at Plateau Station, Antarctica. *Meteorological Studies at Plateau Station,* J. A. Businger, Ed., Research Series, Vol. 25, Amer. Geophys. Union, 41–73.

Liljequist, G. H., 1956: Energy exchange over an Antarctic snow field: Shortwave radiation. Vol. 2, *Norwegian, British, Swedish Antarctic Expedition, 1949–1952,* Norsk Polarinstitutt.

Ohmura, A., and Coauthors,1998: Baseline Surface Radiation Network (BSRN/WRMC): New precision radiometry for climate research. *Bull. Amer. Meteor. Soc.,* **79,** 2115–2136.

Reijmer, C. H., and J. Oerlemans, 2002: Temporal and spatial variability of the surface energy balance in Dronning Maud Land, East Antarctica. *J. Geophys. Res.,* **107,** 4759, doi:10.1029/2000JD000110.

Renfrew, I. A., and P. S. Anderson, 2002: The surface climatology of an ordinary katabatic wind regime in Coats Land, Antarctica. *Tellus,* **54A,** 464–484.

Stearns, C. R., and G. Wendler, 1988: Research results from Antarctic automatic weather stations. *Rev. Geophys.,* **26,** 45–61.

van den Broeke, M. R., J.-G. Winther, E. Isaksson, J. F. Pinglot, L. Karlöf, T. Eiken, and L. Conrads, 1999: Climate variables along a traverse line in Dronning Maud Land, East Antarctica. *J. Glaciol.,* **45,** 295–302.

——, D. van As, W. Boot, and H. Snellen, cited 2002: EPICA-Netherlands Atmospheric Boundary Layer Experiment (ENABLE) 2001/02 field report. Institute for Marine and Atmospheric Research, Utrecht University. [Available online at http://www.phys.uu.nl/~wwwimau/research/home.html.]

——, ——, and ——, 2004: The surface radiation balance in Antarctica using AWS. *J. Geophys. Res.,* **109,** D09103, doi:10.1029/2003JD004394.

van de Wal, R. S. W., and J. Oerlemans, 1997: Modeling the short-term response of the Greenland ice sheet to global warming. *Climate Dyn.,* **13,** 733–744.

Walden, V. P., S. G. Warren, and F. J. Murcray, 1998: Measurements of the downward longwave radiation spectrum over the Antarctic plateau and comparisons with a line-by-line radiative transfer model for clear skies. *J. Geophys. Res.,* **103,** 3825–3846.

Wilber, A. C., D. P. Kratz, and S. K. Gupta, 1999: Surface emissivity maps for use in satellite retrievals of longwave radiation. NASA Tech. Rep. 1999-209362, 35 pp. [Available online at http://techreports.larc.nasa.gov/ltrs/PDF/1999/tp/NASA-99-tp209362.pdf.]

Wiscombe, W. J., and S. G. Warren, 1980: A model for the spectral albedo of snow. I: Pure snow. *J. Atmos. Sci.,* **37,** 2712–2733.